PERGAMON

International Journal of Heat and Mass Transfer 42 (1999) 2299–2311

International Journal of HEAT and MASS TRANSFER

A general modeling for heat transfer during reflux condensation inside vertical tubes surrounded by isothermal fluid

Gung-Huei Chou*, Jyh-Chen Chen

Department of Mechanical Engineering, National Central University, Chung-Li, Taiwan 32054, Republic of China

Received 20 May 1997

Abstract

An analytical modeling of condensation heat transfer characteristics under reflux cooling mode inside vertical tubes surrounded by isothermal external fluid was conducted in the present work. The dimensionless film thickness, film Reynolds number as well as the heat transfer coefficient in the condensate film were formulated and calculated numerically. The results indicate that the increase in Biot number thickens the film layer, speeds the film Reynolds number, and increases the condensation heat transfer coefficient. As $Bi \gg 1$ and $\hat{N}u = 1$, the limiting cases for both isothermal wall and uniform wall heat flux, respectively, were derived for comparison. As compared with the experimental data of reflux condensation from previous studies, the analytical results show good agreement with the observed trend of the condensation heat transfer.

Nomenclature

B $(1+2F)^{1/2}$
Bi Biot number, $h_e\delta_0/k_l$
c_{pl} specific heat capacity of the condensate [J kg^{-1} °C^{-1}]
f_i interfacial friction factor
F $P_l\bar{\delta}^3/3$
g gravitational acceleration
G $1+S/2(1/Re_0)(\mathrm{d}Re_\delta^2/\mathrm{d}\bar{x})$
h_{fg} latent heat [J kg^{-1}]
k_l thermal conductivity of the condensate [W m^{-1} °C^{-1}]
Ku Kutateladze number, $c_{pl}(T_s-T_\infty)/h_{fg}$
Nu Nusselt number, $q''/(T_s-T_w)(\delta_0/k_l)$
$\hat{N}u$ Nusselt number, $q''(T_s-T_\infty)(\delta_0/k_l)$
p pressure [N m^{-2}]
$\bar{p}$ non-dimensional pressure, $p/\rho_l u_0^2$
Pe Peclet number for the condensate film, $Pr\,Re_0$
Pr Prandtl number for the condensate film, $\mu_l/c_{pl}k_l$
P_l $f_iS\,Re_0$
q'' heat flux at the inner wall of the tube [W m^{-2}]
r radial coordinate [m]
R inner radius of the tube [m]
$\bar{R}$ non-dimensional inner radius, R/δ_0
Re_δ film Reynolds number, Γ/μ_l
Re_0 Reynolds number, $\rho_l u_0\delta_0/\mu_l$
S $4\rho_l/(\rho_v\bar{R}^2)$
T_l condensate film temperature [°C]
$\bar{T}_l$ non-dimensional condensate film temperature, $(T_l-T_{sat})/(T_{sat}-T_\infty)$
T_{sat} vapor saturation temperature [°C]
T_w wall temperature [°C]
T_∞ temperature of external fluid environment [°C]
u_l axial condensate velocity [m s^{-1}]
u_v axial steam velocity [m s^{-1}]
$\bar{u}_l$ non-dimensional axial condensate velocity, u_l/u_0
u_{li} interfacial condensate film velocity [m s^{-1}]
$\bar{u}_{li}$ non-dimensional interfacial condensate film velocity
u_0 interfacial condensate film velocity with no interfacial drag [m s^{-1}]
v_l transversal condensate film velocity [m s^{-1}]
$\bar{v}_l$ non-dimensional transversal condensate film velocity, v_l/u_0
x axial coordinate [m]
$\bar{x}$ non-dimensional axial coordinate, x/δ_0
y transversal coordinate [m]

* Corresponding author. Current address: Institute of Nuclear Energy Research, P.O. Box 3-3, Lung-tan 325, Taiwan. Tel.: 00886 3 4711400; fax: 00886 3 4711404; e-mail: ghchou@iner.aec.gov.tw

0017–9310/99/$ - see front matter
PII: S0017–9310(98)00316–0

$\bar{y}$ non-dimensional transversal coordinate, y/δ_0.

Greek symbols

γ ρ_v/ρ_l

Γ condensate mass flow rate per unit width [kg m^{-1} s^{-1}]

δ base flow film thickness [m]

$\bar{\delta}$ non-dimensional base flow film thickness, δ/δ_0

δ_0 base flow film thickness at the tube entrance [m]

η non-dimensional transversal coordinate, $\bar{y}/\bar{\delta}$

μ_l absolute viscosity of the condensate film [kg m^{-1} s^{-1}]

μ_v absolute viscosity of the steam [kg m^{-1} s^{-1}]

ρ_l condensate film density [kg m^{-3}]

ρ_v steam density [kg m^{-3}]

σ surface tension.

Subscripts

l liquid phase

li interface of condensate film and steam

v vapor phase.

1. Introduction

The small-break loss-of-coolant accident (LOCA) is a problem of frequent concern for nuclear safety analysis of a pressurized water reactor (PWR), the reactor coolant pump should have to trip when the primary system pressure is less than a predetermined setpoint, and hence, natural circulation will result. During the cool-down phase, adequate removal of decay heat from the core by the primary coolant must be provided at all times. Several mechanisms and modes of natural circulation of primary core coolant can occur following a small-break LOCA [1]. The reflux condensation process may occur in the vertical steam generator tubes, and the steam generated would condensate on the steam generator tube walls and then run back to the vessel in a countercurrent flow. Therefore, understanding and modeling of this mechanism is of considerable importance in reactor safety analysis.

In the past, many experimental studies were conducted to investigate reflux condensation and flow limiting phenomena in countercurrent liquid–vapor flows by use of two-phase closed thermosyphon or single and/or multiple vertical tubes [2–5]. However, the analytical modeling of reflux condensation was, to the author's knowledge, still scarcely found in the available literature [6–9]. The condensation heat transfer coefficient was investigated both theoretically and experimentally by Tien et al. [6] with special attention given to the effect of interfacial shear stress for constant inner wall temperature. Recently, Girard and Chang [10] presented an extended Nusselt theory and developed an analytical modeling of reflux condensation with constant inner wall heat flux.

In contrast to the limiting situations of uniform wall heat flux and uniform wall temperature, the present study extends the problem to a general case for convective heat transfer from external tube surface to an isothermal fluid environment with uniform heat transfer coefficient h_e and constant temperature T_∞. In the present analysis, similar notations in Girard and Chang's studies were used in the mathematical modeling for comparison. The dimensionless film thickness, heat transfer coefficient as well as the temperature profile and pressure gradient in the condensate film are formulated or calculated numerically further. Furthermore, the present study was extended to derive the limiting cases for both isothermal wall and uniform wall heat flux conditions and the results were compared with previous works reported.

2. Formulation of the problem

The physical mode and the coordinate system are shown in Fig. 1. The saturated vapor flows upward in the tube core and condenses at the tube inner wall. The similar assumptions, as specified by Girard and Chang [10], are made except that the tube is surrounded and cooled by isothermal external fluid. Assuming further that the thermal resistance of the tube wall is comparatively negligible, then the local heat flux may be taken as proportional to the ambient-tube temperature difference

$$q'' = h_e[T_w(x) - T_\infty] \tag{1}$$

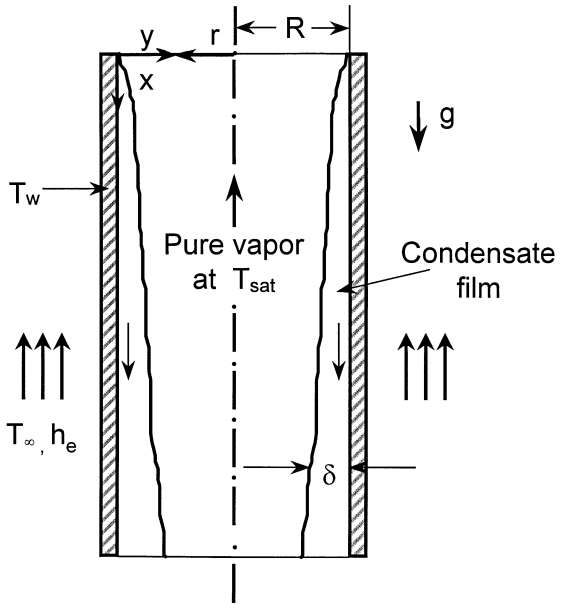

Fig. 1. Physical configuration and the coordinate system of reflux condensation.

where h_e is the external heat-transfer coefficient, assumed known and kept constant.

The geometry of the system being cylindrical, the conservation equations of mass, momentum and energy in both liquid and vapor phases can be described as follows:

Liquid phase:

$$\frac{\partial}{\partial x}(\rho_l r u_l)+\frac{\partial}{\partial r}(\rho_l r v_l)=0 \tag{2}$$

$$\frac{\partial}{\partial x}(\rho_l u_l^2 r)+\frac{\partial}{\partial r}(\rho_l u_l v_l r)=-r\frac{\partial p}{\partial x}+\mu_l\frac{\partial}{\partial r}\left(r\frac{\partial u_l}{\partial r}\right)+gr(\rho_l-\rho_v) \tag{3}$$

$$\frac{\partial}{\partial x}(r\rho_l c_{pl} u_l T_l)+\frac{\partial}{\partial r}(r\rho_l c_{pl} v_l T_l)=k_l\frac{\partial}{\partial r}\left(r\frac{\partial T_l}{\partial r}\right). \tag{4}$$

Vapor phase:

$$\frac{\partial}{\partial x}(\rho_v r u_v)+\frac{\partial}{\partial r}(\rho_v r v_v)=0 \tag{5}$$

$$\frac{\partial}{\partial x}(\rho_v u_v^2 r)+\frac{\partial}{\partial r}(\rho_v u_v v_v r)=-r\frac{\partial p}{\partial x}+\mu_v\frac{\partial}{\partial r}\left(r\frac{\partial u_v}{\partial r}\right) \tag{6}$$

$$T_v=T_s. \tag{7}$$

Under the steady-state assumption, the mass is conserved at each cross-section of the two-phase region, and hence we have

$$\int_{R-\delta(x)}^{R}\rho_l u_l r\,dr=R\Gamma=-\int_0^{R-\delta(x)}\rho_v u_v r\,dr. \tag{8}$$

In the present study, the condensation process occurs in the presence of a body force (gravity) and forced convection of the steam and the condensate at a Prandtl number greater than or equal to one. The condensate and vapor momentum equations from $r=[R-\delta(x)]$ to $r=R$ and from $r=0$ to $r=[R-\delta(x)]$ are integrated, respectively. Summing up these equations, the pressure gradient can be obtained. When substituting the resulting expression for the pressure gradient into the condensate momentum equation and neglecting the inertia terms, the governing equations for the liquid motion can be written as:

$$\mu_l\frac{\partial^2 u_l}{\partial y^2}+g(\rho_l-\rho_v)+\frac{4}{\rho_v R^2}\frac{d}{dx}\Gamma^2=0 \tag{9}$$

with the following boundary conditions:

at $y=0$; $u_l=0$

at $y=\delta$; $\mu_l\dfrac{\partial u_l}{\partial y}=\dfrac{f_i}{2}\rho_v(u_v-u_{li})|u_v-u_{li}|$

where $y=(R-r)$ is the transverse coordinate as shown in Fig. 1, f_i the interfacial friction factor and u_{li} the liquid film velocity at the interface. For pipe flow with no suction, the interfacial friction factor is given by [8]:

$f_i=16/Re_v$, $Re_v<2000$

$f_i=Re_v^{0.33}/1525$, $2000<Re_v<4000$

$f_i=0.079Re_v^{-0.25}$, $4000<Re_v<30\,000$

$f_i=0.046Re_v^{-0.2}$, $30\,000<Re_v<10^6$.

Introducing the following variables for use in non-dimensionalizing the governing equations:

$$\bar\delta=\delta/\delta_0,\quad \bar x=x/\delta_0,\quad \bar y=y/\delta_0 \tag{10}$$

$$\bar u_l=u_l/u_0,\quad \bar v_l=v_l/u_0,\quad \bar T_l=(T_l-T_{sat})/(T_{sat}-T_\infty)$$

and using the boundary conditions, equation (9) can be easily integrated, resulting in the following expression for the liquid velocity:

$$\bar u_l=(2\bar\delta\bar y-\bar y^2)\left(1+\frac{S}{2Re_0}\frac{dRe_\delta^2}{d\bar x}\right)-\frac{Sf_i}{2Re_0}Re_\delta^2\,\bar y. \tag{11}$$

The velocity component in the y-direction can be obtained by using the continuity equation as

$$v_l=-G\frac{d\bar\delta}{d\bar x}\bar y^2-\frac{S}{2Re_0}\frac{d^2Re_\delta^2}{d\bar x^2}\left(\bar\delta\bar y^2-\frac{\bar y^3}{3}\right)+\frac{S\,Re_\delta^2}{4Re_0}\frac{df_i}{d\bar x}\bar y^2+\frac{Sf_i}{4Re_0}\frac{dRe_\delta^2}{d\bar x}\bar y^2. \tag{12}$$

The energy conservation equation for the condensate film in non-dimensional form can be written as:

$$\bar u_l\frac{\partial\bar T_l}{\partial\bar x}+\bar v_l\frac{\partial\bar T_l}{\partial\bar y}=\frac{1}{Pe}\frac{\partial^2\bar T_l}{\partial\bar y^2} \tag{13}$$

with the following boundary conditions:

at $\bar y=0$; $\dfrac{\partial\bar T_l}{\partial y}=Bi(\bar T_l+1)$

at $\bar y=\bar\delta$; $\bar T_l=0$.

The temperature profile of the liquid film can be expressed as

$$\bar T_l=\eta+\bar T_p \tag{14}$$

where $\bar T_p=\bar T_p(\eta)$ is a high-order polynomial and $\eta=\bar y/\bar\delta$ [10]. By using equation (14) and the velocity distributions given by equations (11) and (12) and keeping the first-order term only, the energy equation becomes

$$\frac{d^2\bar T_p}{d\eta^2}=\left[G\eta^3-3G\eta^2+\frac{Sf_i}{2Re_0}\frac{Re_\delta^2}{\bar\delta}\eta^2+\frac{dG}{d\bar\delta}\left(\frac{\eta^3}{3}-\eta^2\right)\bar\delta+\frac{Sf_i}{4Re_0}\frac{dRe_\delta^2}{d\bar\delta}\eta^2\right]\times Pe\,\bar\delta^3\frac{d\bar\delta}{d\bar x} \tag{15}$$

with the following boundary conditions:

at $\eta=0$; $\dfrac{d\bar T_p}{d\eta}=Bi\,\bar\delta(\bar T_l+1)-1$

at $\eta=1$; $\bar T_p=-1$.

Integration of equation (15) with the application of its boundary conditions and simplification by an order of magnitude analysis of the resulting expression yields:

$$\bar{T}_l = \eta + \left[\frac{G}{20}\eta^5 - \left(\frac{G}{4} - \frac{Sf_i}{24Re_0}\frac{Re_\delta^2}{\bar{\delta}} - \frac{Sf_i}{24Re_0}Re_\delta\frac{dRe_\delta}{d\bar{\delta}}\right)\eta^4\right] Pe\,\bar{\delta}^3\frac{d\bar{\delta}}{d\bar{x}} - \left(\frac{Bi\,\bar{\delta}\Phi+1}{Bi\,\bar{\delta}+1}\right)\eta - \frac{Bi\,\bar{\delta}+\Phi}{Bi\,\bar{\delta}+1} \quad (16)$$

where

$$\Phi = \left[-\frac{G}{5} + \frac{Sf_i}{24Re}\left(\frac{Re_\delta^2}{\bar{\delta}} + Re_\delta\frac{dRe_\delta}{d\bar{\delta}}\right)\right] Pe\,\bar{\delta}^3\frac{d\bar{\delta}}{d\bar{x}}.$$

By definition we have:

$$Re_\delta = \frac{\Gamma}{\mu_l} = \int_0^\delta \frac{\rho_l u_l}{\mu_l}dy. \quad (17)$$

Substituting equation (11) into equation (17) we obtain

$$Re_\delta = \frac{\frac{4}{3}Re_0\,\bar{\delta}^3}{1+\sqrt{(1+2F)}} \quad (18)$$

where $F = P_l\bar{\delta}^5/3$. Introducing the equations (16) and (18) with the combination of the heat and mass interfacial jump conditions, the following differential equation for the dimensionless film thickness is obtained:

$$\frac{Pe}{3Ku}\frac{d\bar{\delta}^3}{d\bar{x}} = \frac{Bi}{Bi\,\bar{\delta}+1}\left\{\frac{4}{1+B} - \frac{\frac{20}{3}F}{B(1+B)^2} + Ku\left[\frac{3}{4}G - \frac{\frac{8}{9}F}{(1+B)^2}\left(4-\frac{5F}{B(1+B)}\right) - \frac{Bi\,\bar{\delta}}{Bi\,\bar{\delta}+1}\left(\frac{G}{5} - \frac{\frac{2}{9}F}{(1+B)^2}\left(4-\frac{5F}{B(1+B)}\right)\right)\right]\right\}^{-1} \quad (19)$$

where $B = (1+2F)^{1/2}$. From the momentum equation and the no-slip conditions, the pressure gradient can be written as:

$$\frac{\partial\bar{p}}{\partial\bar{x}} = \frac{S}{Re_0^2}\left(\frac{f_i}{\bar{R}}Re_\delta^2 - \frac{dRe_\delta^2}{d\bar{x}}\right). \quad (20)$$

Attention may now be turned to the heat transfer characteristics. Two definitions of the Nusselt number are examined in the present study [11, 12]:

$$Nu = \frac{q''}{T_{sat}-T_w}\frac{\delta_0}{k_l}, \quad \hat{Nu} = \frac{q''}{T_{sat}-T_\infty}\frac{\delta_0}{k_l} \quad (21)$$

whereas the first of these is the conventional definition for pipe flows, it is not very useful for the case of external cooling since both q'' and T_w are unknowns. The second definition is more of a direct applicability since it contains only q'' as an unknown. From a resistance series argument, the relationship between Nu and $\hat{Nu}$ is readily deduced as

$$\frac{1}{\hat{Nu}} = \frac{1}{Nu} + \frac{1}{Bi} \quad (22)$$

where $Bi = h_e\delta_0/k_l$ is the Biot number. The first boundary condition of equation (13) is the statement of heat flux continuity through the wall surface ($y = 0$). That is

$$q'' = k_l\left(\frac{\partial T_l}{\partial y}\right) = h_e(T_w - T_\infty) \quad \text{at } y = 0. \quad (23)$$

Thus, the $\hat{Nu}$ definition from equation (21) yields

$$\frac{\partial\bar{T}_l}{\partial\bar{y}} = \hat{Nu} \quad \text{at } \bar{y} = 0. \quad (24)$$

Integrating equation (15) with the application of the boundary condition equation (24), we have:

$$\hat{Nu} = \frac{Bi}{Bi\,\bar{\delta}+1}\left\{1 + \frac{Pe}{4}\frac{d\bar{\delta}^4}{d\bar{x}} \times\left[\frac{1}{5} - \frac{F}{9(1+B)^2}\left(8 - \frac{10F}{B(1+B)}\right)\right]\right\}. \quad (25)$$

3. Numerical results

The present study developed a general expression for the heat transfer characteristics during reflux condensation inside vertical tubes by isothermal external fluid. To take it one step further, the authors extended the present results to derive the limiting cases for both isothermal wall and uniform wall heat flux. By examining the boundary conditions at the wall in the energy equation among the limiting cases and the present study, the relations were found. When the external thermal contact is superior, $h_e\delta_0/k_l \gg 1$ (i.e., $Bi \gg 1$), the wall temperature T_w approaches the isothermal condition $T_w = T_\infty =$ constant, which is the limiting case of the isothermal wall condition. While the uniform wall heat flux is the limiting case of the present study when $\hat{Nu} = 1$. For $Bi \gg 1$, equations (16), (19) and (25) are simplified as follows:

$$\bar{T}_l = \eta - 1 + \left\{\frac{G}{20}(\eta^5-\eta) - \frac{G}{4}(\eta^4-\eta) + \left[\frac{Sf_i}{24Re_0}\frac{Re_\delta^2}{\bar{\delta}} + \frac{Sf_i}{24Re_0}(Re_\delta)\left(\frac{dRe_\delta}{d\bar{\delta}}\right)\right](\eta^4-\eta)\right\} \times Pe\,\bar{\delta}^3\frac{d\bar{\delta}}{d\bar{x}} \quad (26)$$

$$\frac{Pe}{4Ku}\frac{d\bar{\delta}^4}{d\bar{x}} = \left\{\frac{4}{1+B} - \frac{\frac{20}{3}F}{B(1+B)^2} + Ku\left[\frac{11}{20}G - \frac{\frac{2}{3}F}{(1+B)^2}\left(4-\frac{5F}{B(1+B)}\right)\right]\right\}^{-1} \quad (27)$$

$$\hat{Nu} = Nu = \frac{1}{\bar{\delta}}\left\{1+\frac{Pe}{4}\frac{d\bar{\delta}^4}{d\bar{x}} \times\left[\frac{1}{5}-\frac{F}{9(1+B)^2}\left(8-\frac{10F}{B(1+B)}\right)\right]\right\}. \quad (28)$$

Similarly, as $\hat{Nu}=1$, we can also obtain the following results for the uniform wall heat flux limit by substituting equation (25) into equations (16) and (19):

$$\bar{T}_l = \bar{\delta}(\eta-1)+\left\{\frac{G}{20}(\eta^5-1)-\frac{G}{4}(\eta^4-1)+\left[\frac{Sf_i}{24Re_0}\frac{Re_\delta^2}{\bar{\delta}} + \frac{Sf_i}{24Re_0}(Re_\delta)\left(\frac{dRe_\delta}{d\bar{\delta}}\right)\right](\eta^4-1)\right\}\times Pe\,\bar{\delta}^3\frac{d\bar{\delta}}{d\bar{x}} \quad (29)$$

$$\frac{Pe}{3Ku}\frac{d\bar{\delta}^3}{d\bar{x}} = \left\{\frac{4}{1+B}-\frac{\frac{20}{3}F}{B(1+B)^2} + Ku\left[\frac{3}{4}G-\frac{\frac{8}{9}F}{(1+B)^2}\left(4-\frac{5F}{B(1+B)}\right)\right]\right\}^{-1} \quad (30)$$

$$\hat{Nu}=1. \quad (31)$$

Equations (26)–(31), for the typical cases when $Bi \gg 1$ and $\hat{Nu}=1$, were already derived in our previous study [13]. As $Bi \to 0$ (i.e., $h_e \approx 0$) for the adiabatic condition, the following equations can also be obtained from the present results:

$$\bar{T}_l = \left\{\frac{G}{20}(\eta^5-1)-\frac{G}{4}(\eta^4-1) + \left[\frac{Sf_i}{24Re_0}\frac{Re_\delta^2}{\bar{\delta}}+\frac{Sf_i}{24Re_0}(Re_\delta)\left(\frac{dRe_\delta}{d\bar{\delta}}\right)\right](\eta^4-1)\right\} \times Pe\,\bar{\delta}^3\frac{d\bar{\delta}}{d\bar{x}} \quad (32)$$

$$\bar{\delta} = \text{constant} \quad (33)$$

$$\hat{Nu}=0. \quad (34)$$

It is interesting to note that the behavior of equations (27) and (30) as the interfacial shear goes to zero, or in mathematical terms as F goes to zero, we can obtain the following results for both the limiting cases of isothermal wall (IW) and uniform heat flux (UHF):

IW:

$$\lim_{F\to 0}\frac{d\bar{\delta}^4}{d\bar{x}} = \frac{4Ku}{Pe}\left(2+\frac{11}{20}Ku\right)^{-1}. \quad (35)$$

UHF:

$$\lim_{F\to 0}\frac{d\bar{\delta}^3}{d\bar{x}} = \frac{3Ku}{Pe}\left(2+\frac{3}{4}Ku\right)^{-1}. \quad (36)$$

Here, $Ku = c_{pl}(T_s-T_\infty)/h_{fg}$ is the Kutateladze number. If the condensation process is slow ($Ku \ll 1$), integrating equations (35) and (36) with the application of the initial condition of $\bar{\delta}=0$ at $\bar{x}=0$ and the definitions of Ku, Re_0, and Pr gives the results for the dimensional film thickness as reported by Nusselt and the other investigators [14]:

IW:

$$\delta(x) = \left[\frac{4\mu_l k_l x(T_{sat}-T_w)}{g\rho_l^2 h_{fg}}\right]^{1/4}. \quad (37)$$

UHF:

$$\delta(x) = \left[\frac{3q''\mu_l x}{g\rho_l^2 h_{fg}}\right]^{1/3}. \quad (38)$$

The agreement of equations (37) and (38) with results found in the open literature may be used to check the validity of the present mathematical model of reflux condensation.

For a sufficiently long vertical tube, $P_l\bar{\delta}^5$ is larger than unity (i.e., $F \gg 1$). Then equations (18), (27), (28) and (30) can be integrated from the initial condition of $\bar{\delta}=0$ at $\bar{x}=0$ and written as follows:

IW:

$$\bar{\delta} = 2.991\left[\frac{1}{Ku}\left(\frac{\bar{x}\,Ku}{Pe}\right)\right]^{1/4} \quad (39)$$

$$\frac{Re_\delta}{Re_0} = 2.824\left[\frac{1}{P_l^4\,Ku}\left(\frac{\bar{x}\,Ku}{Pe}\right)\right]^{1/8} \quad (40)$$

$$\hat{Nu} = 0.557\left[\frac{1}{Ku}\left(\frac{\bar{x}\,Ku}{Pe}\right)\right]^{-1/4}. \quad (41)$$

UHF:

$$\bar{\delta} = 3.302\left[\frac{1}{Ku}\left(\frac{\bar{x}\,Ku}{Pe}\right)\right]^{1/3} \quad (42)$$

$$\frac{Re_\delta}{Re_0} = 2.967\left[\frac{1}{P_l^3\,Ku}\left(\frac{\bar{x}\,Ku}{Pe}\right)\right]^{1/6} \quad (43)$$

$$\hat{Nu}=1. \quad (44)$$

4. Discussions

Previous theoretical analyses of film condensation have mostly been focused on isothermal wall and uniform heat flux limits. In contrast to these limiting situations, the present study extends the problem to a general case which is more practical. In summary, equations (8), (16), (18)–(20), and (25) are the governing equations of the present model to describe the behaviors for reflux condensation of a countercurrent two-phase flow, equations (19) and (25) cannot be integrated analytically. Consequently, they are numerically integrated by using a fourth-order Runge–Kutta scheme. For the selected values of Ku ($=0.05$ and 0.0) and P_l ($=0.01$), the dimensionless film thickness ($\bar{\delta}$), liquid film Reynolds number (Re_δ/Re_0) and local film Nusselt number ($\hat{Nu}$) are calculated and plotted as functions of $\bar{x}\,Ku/Pe$ with different Biot numbers.

Figures 2 and 3 illustrate the dimensionless film thickness variations along the tube cooled by isothermal fluid with different Biot numbers for selected values of Ku and P_l. In Fig. 2, it indicates that the dimensionless film thickness $\bar{\delta}$ increases with increasing Bi, and the rate of increase is larger for longer condensation length, so that the dimensionless film thickness tends to approach an asymptotic relation independent of Bi if the tube has a sufficiently long condensation length. It has also seen from Fig. 2 that $\bar{\delta}$ changes with very little difference as $Bi \gg 1$. The result approaches to the limiting case of the isothermal wall. For the case of uniform heat flux limit, the rate of the variations in $\bar{\delta}$ is evidently larger in the shorter condensation length. The relations given by equations (39) and (42) for both IW and UHF cases with a sufficiently long vertical tube, respectively, are also shown in Fig. 2 by chain-dotted lines which are independent of P_l or the interfacial shear stress. The prediction for $Ku = 0$ (no convection) is shown in Fig. 3, the variation of $\bar{\delta}$ vs $\bar{x}\,Ku/Pe$ results for different Bi are similar to that in the case of $Ku = 0.05$, but the increase rate of $\bar{\delta}$ varies drastically for the case of the uniform heat flux limit. It is concluded that the interfacial shear thickens the film relatively more pronounced for the UHF case, especially when the convection effect is neglected.

The variation of the film Reynolds number Re_δ/Re_0 along the tube length is shown in Fig. 4, the film Reynolds number increases with increasing Bi, and the film Reynolds number will approach to an asymptotic relation independent of Bi. It is worth noting, as shown from Fig. 4, that the film Reynolds number changes with very little difference as $Bi \gg 1$, and approaches to the limiting case of the isothermal wall. For the case of uniform heat flux limit, the rate of the variations in Re_δ/Re_0 is evidently larger along the condensation length. The relations of the film Reynolds numbers given by equations (40) and (43) for both IW and UHF cases, respectively, are also plotted in Fig. 4, the results show good approach in the large $\bar{x}\,Ku/Pe$ region. This can further validate the numerical results of the present mathematical modeling. The results

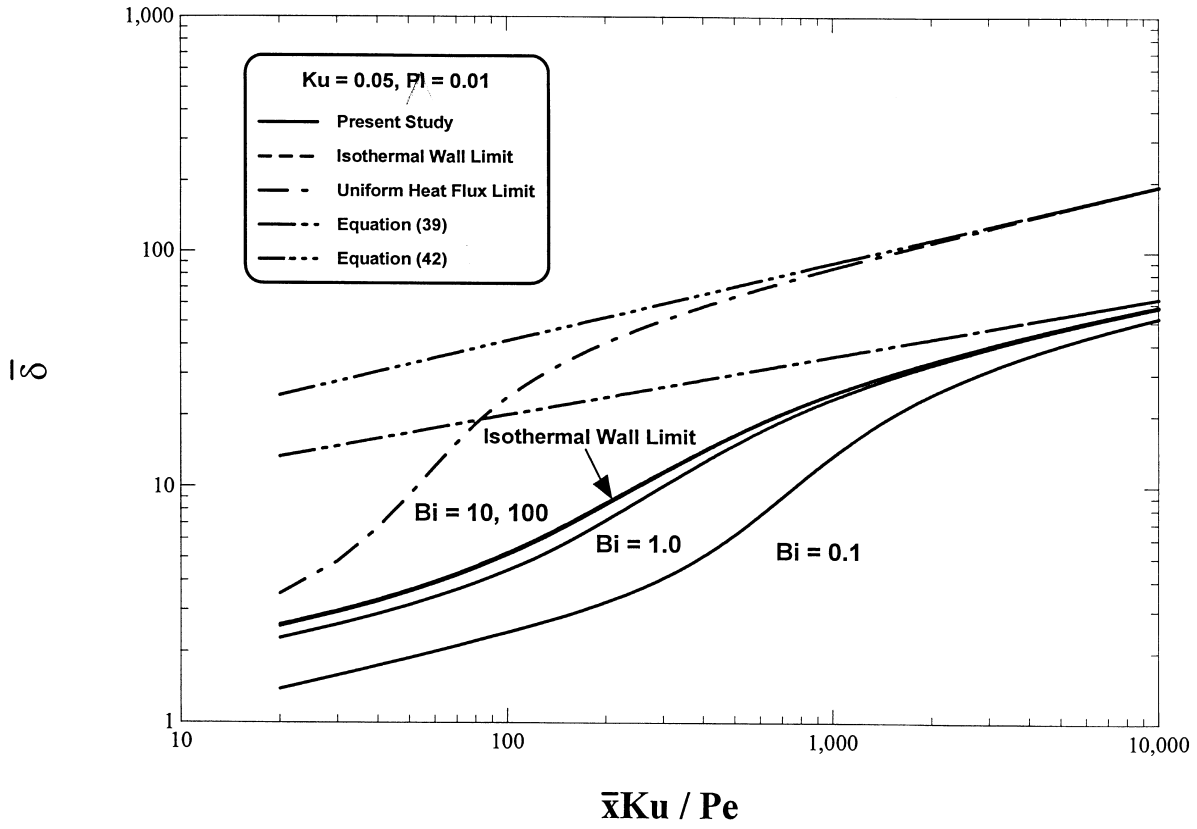

Fig. 2. The dimensionless film thickness variation as functions of the dimensionless tube length with different Biot numbers for $Ku = 0.05$, $P_l = 0.01$.

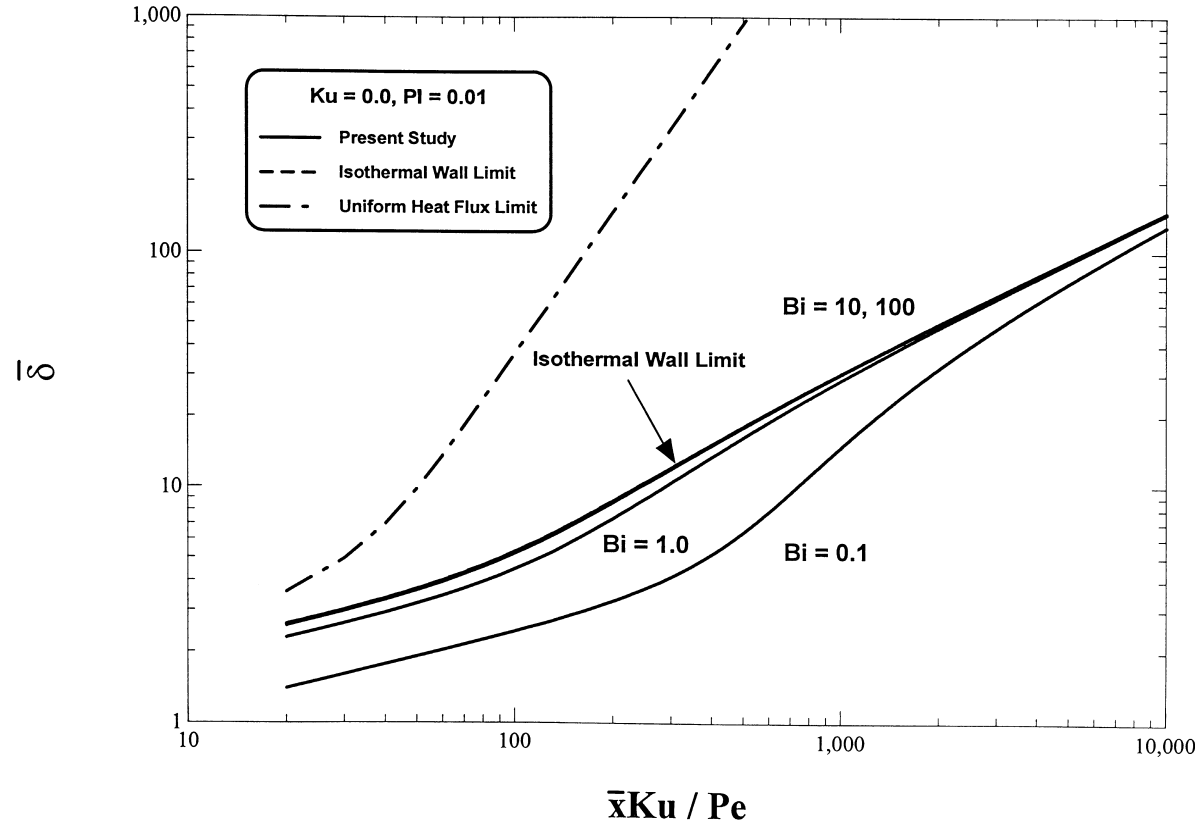

Fig. 3. The dimensionless film thickness variation as functions of the dimensionless tube length with different Biot numbers for $Ku = 0.0$, $P_l = 0.01$.

for $Ku = 0$ are shown in Fig. 5, the variation of the film Reynolds number Re_δ/Re_0 along the tube length for the UHF case varies almost linearly and is more drastic.

The heat transfer results for the selected values of Ku and P_l are shown as Fig. 6 and 7 for comparison. The heat transfer coefficient $\hat{N}u$ increases with increasing Bi, and decreases along the tube length. When the tube has a sufficiently long condensation length, the local film Nusselt number approaches to an asymptotic relation independent of Bi. For $Bi > 10$, the result approaches also to the limiting case of the isothermal wall. The relation given by equation (41) is shown in Fig. 6 by a chain-dotted line, which is independent of P_l. In the UHF case, the local film Nusselt number, as derived in equation (31), keep unity along the tube length which is independent of P_l and Ku. The calculation results for $Ku = 0$ (no convection) are depicted in Fig. 7 to clarify the effect of convection in the liquid film on the heat transfer coefficient. The zero-convection result causes a noticeable decrease in $\hat{N}u$ in comparison with the non-zero convection case, especially in the large $\bar{x}\,Ku/Pe$ region. Besides, Fig. 7 also illustrates that the local film Nusselt number for large Bi is lower than that for small Bi at certain condensation length. This is due to the fact that, for large Bi, higher film Reynolds number and larger film thickness are present in the large $\bar{x}\,Ku/Pe$ region. The resulting increase in the thermal resistance of the film tends to depress heat transfer.

Equation (18) represents the relation between $\bar{\delta}$ and Re_δ with the functional form $\bar{\delta} = f(P_l, Re_\delta)$. The variation of the dimensionless film thickness $\bar{\delta}$ as functions of the dimensionless film Reynolds number Re_δ/Re_0 with different values of P_l is shown in Fig. 8. It depicts that $\bar{\delta}$ increases with increasing P_l and the rate of increase is larger in higher Re_δ. Large condensate flow would exert high interfacial shear stress upon the liquid layer, and hence, thickens the film thickness. Furthermore, the result indicates that $\bar{\delta}$ varies with Re_δ/Re_0 independently not only for the different values of Bi, but for the different thermal boundary conditions in the present study. Figure 9 illustrates the local film Nusselt number variation as functions of the dimensionless film Reynolds number for

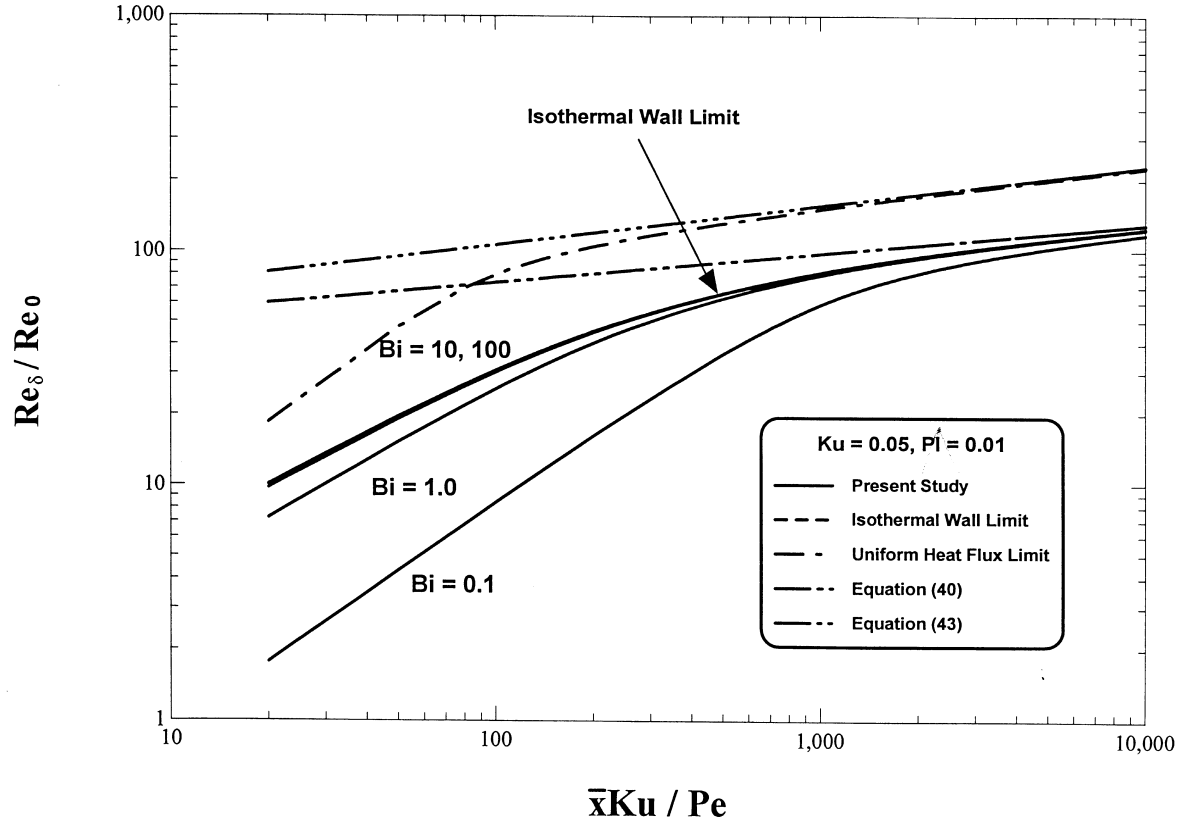

Fig. 4. The dimensionless film Reynolds number variation as functions of the dimensionless tube length with different Biot numbers for $Ku = 0.05$, $P_1 = 0.01$.

both $Ku = 0.05$ and $Ku = 0$ cases with fixed P_1. The heat transfer coefficient $\hat{N}u$ increases with increasing Bi, and decreases with increasing Re_δ. The results indicate that $\hat{N}u$ changes with very little difference between the non-zero and zero-convection cases. For higher Re_δ, the local film Nusselt number approaches an asymptotic relation independent of Bi and Ku, which presents similar results as described above.

In the open literature, it is difficult to acquire the experimental data conducted for the reflux condensation phenomena inside vertical tubes surrounded by isothermal external fluid. Thus, some experimental data from Chen et al. [8] and Gerner and Tien [16] for constant tube inner wall temperature were collected to compare with the analytical results of the present modeling. As shown in Fig. 10, the experimental data (for both methanol and water) of Chen et al. [8] and Tien et al. [15] and the present model for $Bi = 100$ (i.e., the isothermal wall limit case) are plotted along with the Nusselt prediction. It delineates that the experimental data are quite scattered at low film Reynolds numbers region. It appears that at moderate film Reynolds numbers ($10 < Re_\delta < 50$), the experimental heat transfer coefficients are slightly higher than the Nusselt's solution and the present results. The observed higher values of heat transfer coefficients may be attributed partly to the presence of waviness on the film surface and partly to the effect of liquid carry-over. This increase is offset by the interfacial shear due to the higher vapor flowrates at relatively high film Reynolds numbers. Consequently, the present model which accounts for the interfacial shear stress can achieve better agreement than that predicted by the Nusselt theory. The condensation heat transfer coefficients for $Re_\delta > 100$ are underpredicted in the present model. Both Chen's and Tien's models [8, 15] are presented in Fig. 10 for comparison. Chen et al. improved the theoretical Nusselt's solution, also taking into account the effect of interfacial shear stress, their model underpredicts the experimental data for the selected film Reynolds numbers ranging from 0–60. On the other hand, the correlation proposed by Tien et al. [15] overpredicts the experimental data. This is because Tien's correlation [15] combines both the

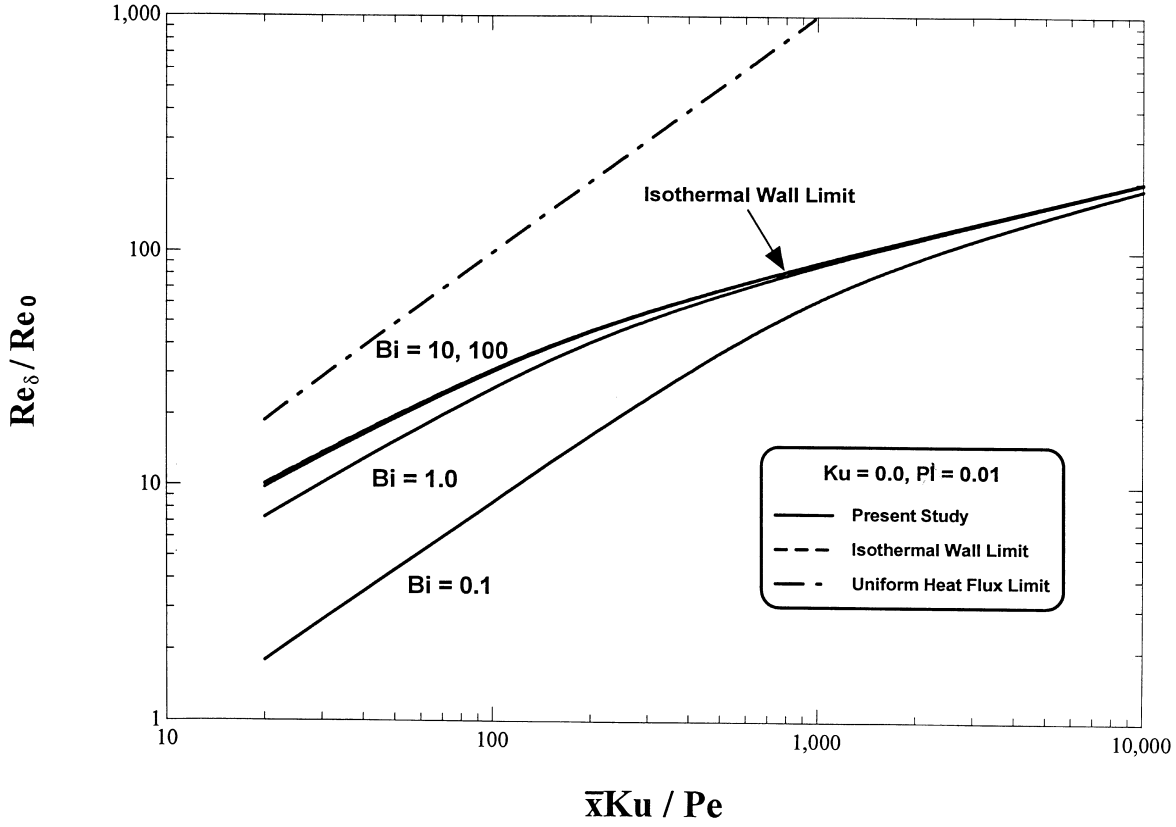

Fig. 5. The dimensionless film Reynolds number variation as functions of the dimensionless tube length with different Biot numbers for $Ku = 0.0$, $P_1 = 0.01$.

effects of interfacial shear stress and waviness. In fact, the interfacial waviness tends to enhance heat transfer which is not so evident as in the experimental results when the film Reynolds numbers are small.

In an inverted U-tube steam generator, the secondary side fluid environment is usually considered as isothermal in heat transfer analysis. Thus, the improved understanding developed in the present study is more practical than the previous researches in either uniform heat flux or isothermal wall cases. Given the geometry of a tube and the proper boundary conditions, pertinent to steam generators, the present model could be applied to compute for the base flow characteristics of a given inlet steam mass flow rate using the extended Nusselt theory plus global mass and energy balances. Furthermore, the results of the present work could be extended for a tube bundle and used in a small-break LOCA analysis to estimate for the heat removal capabilities (via the condensation rates), if, to be conservative, total reflux condensation is the assumed flow regime in each tube of the steam generators.

5. Conclusions

A general analytical modeling of condensation heat transfer characteristics, under reflux cooling modes in a single vertical tube surrounded by isothermal external fluid, was developed in the present study. As $Bi \gg 1$ and $\hat{N}u = 1$, the limiting cases for both isothermal wall and uniform wall heat flux, respectively, were derived for comparison.

The dimensionless film thickness, film Reynolds number, and local film Nusselt number were calculated numerically using a fourth-order Runge–Kutta scheme. The effects of different Biot numbers on the reflux condensation heat transfer are examined. As a result, the increase in the Biot number thickens the film layer, speeds the film Reynolds number, and increases the condensation heat transfer coefficient. For a sufficiently long condensation length, each parameter ($\bar{\delta}$, Re_δ/Re_0 and $\hat{N}u$) approaches an asymptotic relation, respectively, independent of Bi. It is seen that in small condensation length the convection effect on condensation is small. However,

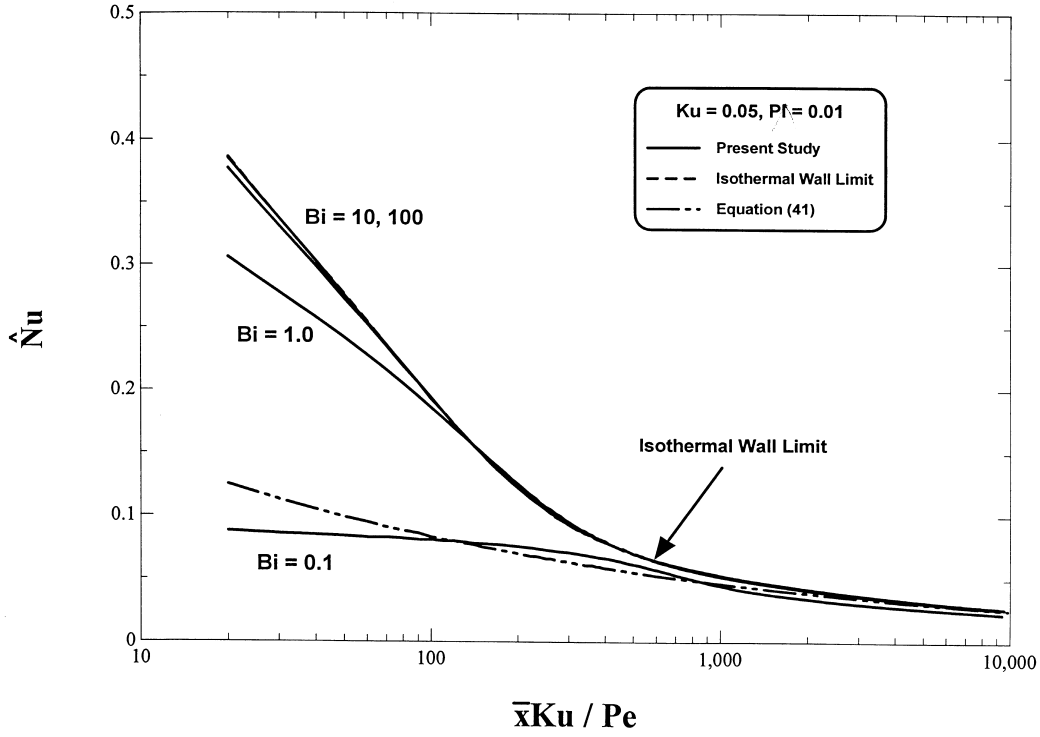

Fig. 6. The local film Nusselt number variation as functions of the dimensionless tube length with different Biot numbers for $Ku = 0.05$, $P_1 = 0.01$.

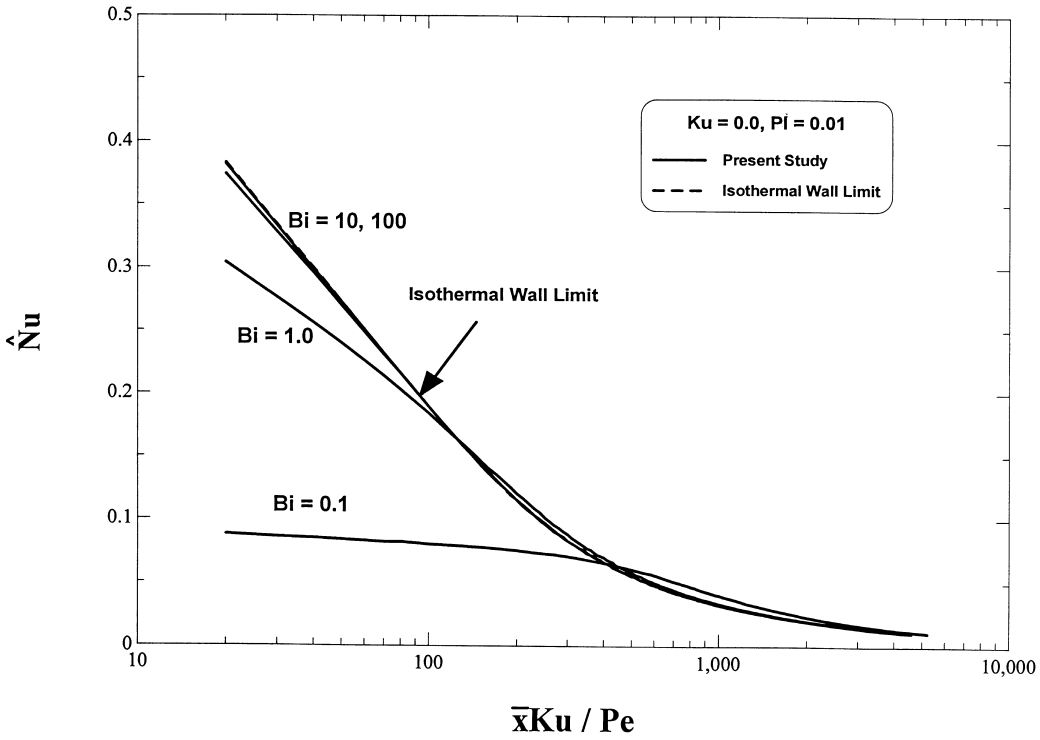

Fig. 7. The local film Nusselt number variation as functions for the dimensionless tube length with different Biot numbers for $Ku = 0.0$, $P_1 = 0.01$.

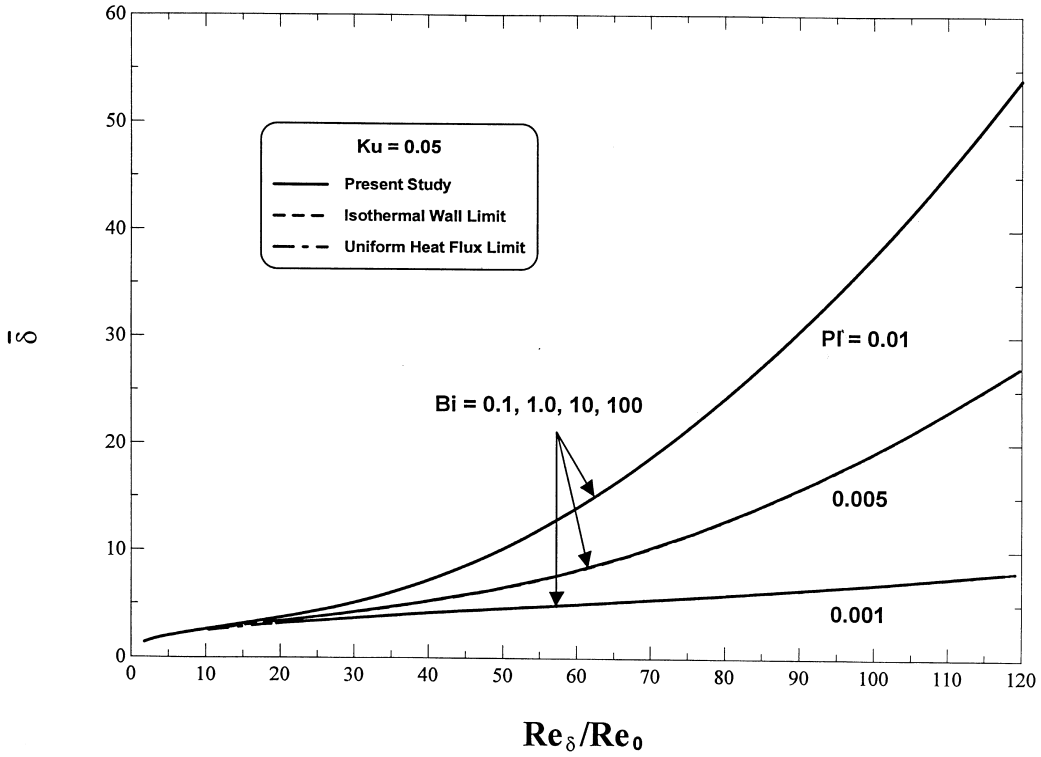

Fig. 8. The dimensionless film thickness variation as functions of the dimensionless film Reynolds number with different Biot numbers for $Ku = 0.05$, and $P_l = 0.01$, 0.005, 0.001.

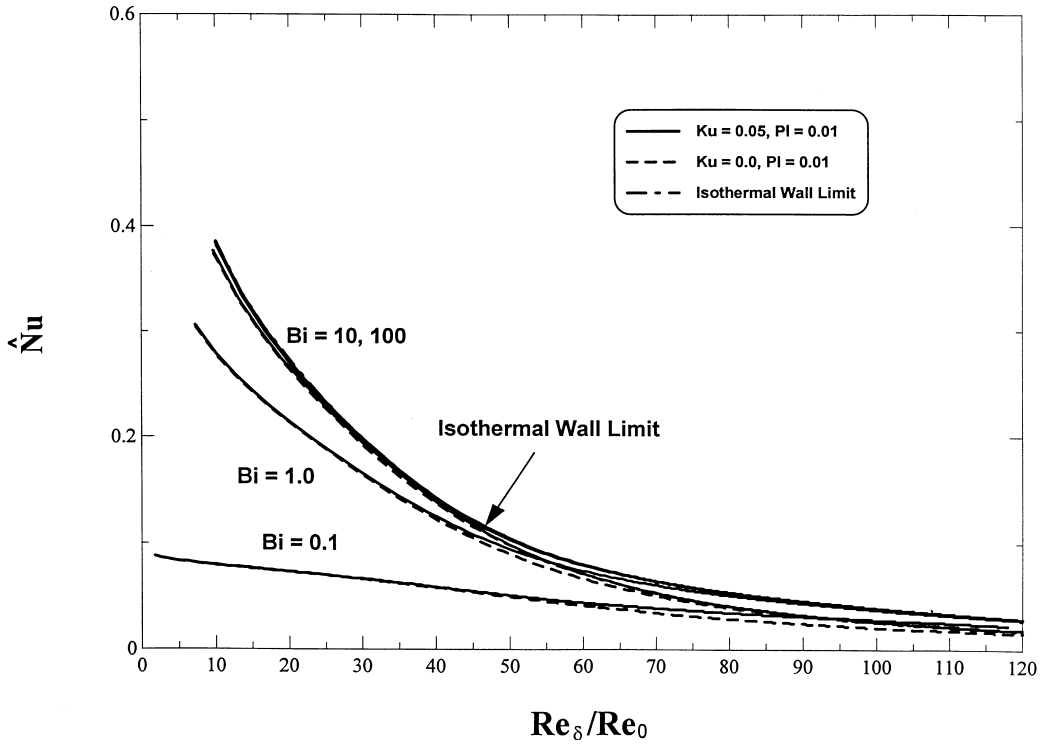

Fig. 9. The local film Nusselt number variation as functions of the dimensionless film Reynolds number with different Biot numbers for $Ku = 0.05$, 0.0, and $P_l = 0.01$.

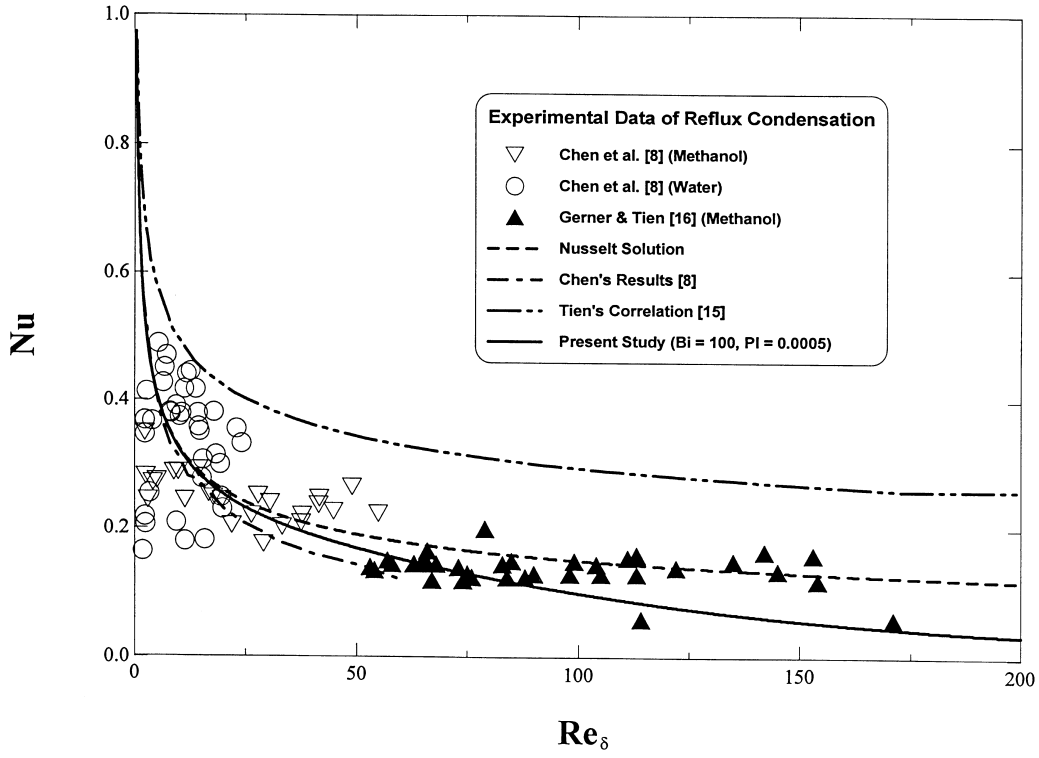

Fig. 10. Comparison of the analytical results with the experimental data of reflux condensation.

it becomes relatively appreciable in the large $\bar{x}\,Ku/Pe$ region. Both $\bar{\delta}$ and Re_δ increase along with the tube condensation length, while $\hat{N}u$ decreases along it. The predicting results indicate that the values of $\bar{\delta}$ and Re_δ at a fixed condensation length for the UHF case are higher than those in the other cases. The result of the isothermal wall case is quantitatively achieved from the present study when larger Bi (>10) is taken into account.

The present analytical results and that of Chen's and Tien's models were compared with the experimental data collected from some open literature. The present model shows good agreement with the observed trend of the condensation heat transfer. The observed higher values of heat transfer coefficients at low film Reynolds numbers region may be attributed partly to the presence of waves on the film surface and partly to the effect of liquid carry-over which were not taken into consideration in the present study.

References

[1] W.E. Burchill, Physical phenomena of small-break loss-of-coolant accident in a PWR, Nuclear Safety 23 (1982) 525–536.

[2] C. Calia, P. Griffith, Modes of circulation in an inverted U-tube array with condensation, ASME J. Heat Transfer 104 (1982) 769–773.

[3] S. Banerjee, J.S. Chang, R. Girard, V.S. Krishnan, Reflux condensation and transition to natural circulation in a vertical U-tube, ASME J. Heat Transfer 105 (1983) 719–727.

[4] Q. Nguyen, S. Banerjee, Analysis of experimental data on condensation in an inverted U-tube, EPRI Report No. NP-4091, Electric Power Research Institute, 1985.

[5] G.F. De Santi, F. Mayinger, Steam condensation and liquid holdup in steam generator U-tubes during oscillatory natural circulation, Experimental Heat Transfer 6 (1993) 367–387.

[6] C.L. Tien, T. Fukano, K. Hijikata, S.J. Chen, Reflux condensation and operating limits of countercurrent vapor–liquid flows in a closed tube, EPRI Report No. NP-2648, Electric Power Research Institute, 1982.

[7] R.A. Seban, J.A. Hodgson, Laminar film condensation in a tube with upward vapor flow, Int. J. Heat Mass Transfer 25(9) (1982) 1291–1300.

[8] S.J. Chen, J.G. Reed, C.L. Tien, Reflux condensation in a two-phase closed thermosyphon, Int. J. Heat Mass Transfer 27(9) (1984) 1587–1594.

[9] J.G. Reed, C.L. Tien, Modeling of the two-phase closed thermosyphon, ASME J. Heat Transfer 109 (1987) 722–730.

[10] R. Girard, J.S. Chang, Reflux condensation phenomena in single vertical tubes, Int. J. Heat Mass Transfer 35(9) (1992) 2203–2217.

[11] E.M. Sparrow, S.V. Patankar, Relationships among boundary conditions and Nusselt numbers for thermally developed duct flows, ASME J. Heat Transfer 99 (1977) 483–485.
[12] A. Bejan, Convective Heat Transfer, John Wiley and Sons, New York, 1984, pp. 82–94.
[13] G.H. Chou, J.C. Chen, Heat transfer characteristics of reflux condensation phenomena in single vertical tube, Nuclear Science and Engineering 127(2) (1997) 220–229.
[14] T. Fujii, H. Uehara, K. Oda, Filmwise condensation on a surface with uniform heat flux and body force convection, Heat Transfer Res. Japan 1 (1972) 76–83.
[15] C.L. Tien, S.L. Chen, P.F. Peterson, Condensation inside tubes, EPRI Report No. NP-5700, Electric Power Research Institute, 1988.
[16] F.M. Gerner, C.L. Tien, Effects of high interfacial shear stress due to countercurrent vapor flow on film condensation heat transfer, Preprint 7th Int. Heat Pipe Conf., Minsk, 1990.